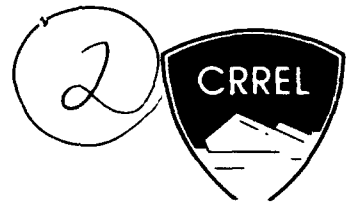


93-15

CRREL REPORT

S DTIC
ELECTE
NOV 29 1993
A



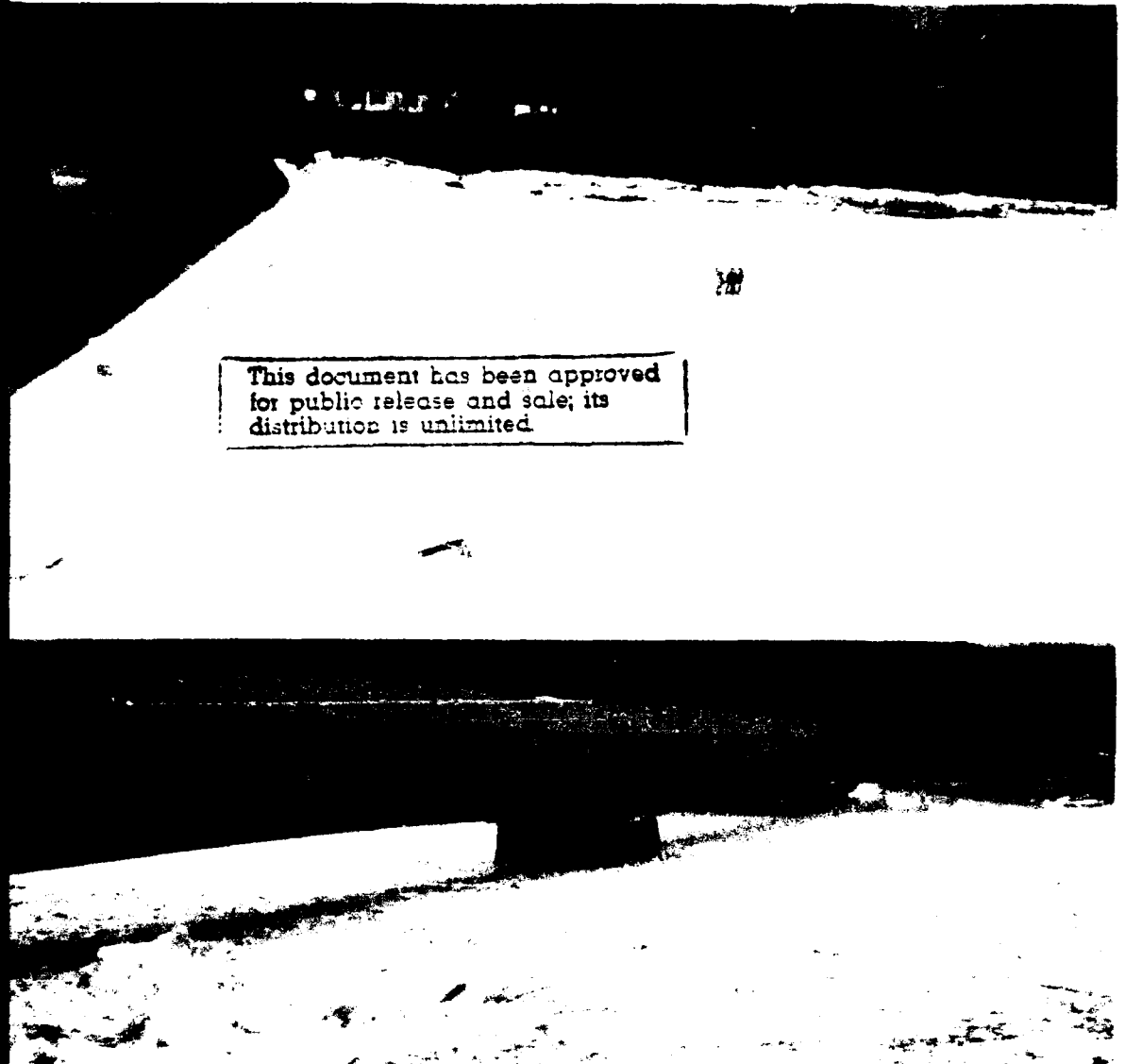
AD-A273 141



Kinematic Model of River Ice Motion During Dynamic Breakup

Michael G. Ferrick, Patricia B. Weyrick and David F. Nelson

September 1993



This document has been approved for public release and sale; its distribution is unlimited.

93-28964



288

93 11 26 008

Abstract

We begin a study of the dynamics of ice motion during river breakup by formulating a kinematic model. Ice continuity equations are applied to relate the speeds of a breaking front, convergence front, stoppage front, and release front with the ice discharge and volume per unit surface area (unit volume) on either side of each front. Ice velocity data are obtained from measurements with time made during a dynamic breakup at a pair of sites bounding a reach of the Connecticut River. We simulate the ice and front motion through time for this reach using the kinematic model with the assumptions that accumulation thickness and porosity are uniform, and that changes in the ice conditions and motion occur only at a front. Contrary to the basic assumption of static jam formation, we find that the accumulation develops while the ice is moving, and that jam formation merely represents the arrest of the motion.

Cover: (Top) Setup of targets on a known grid for video ice velocity measurement at site D on the Connecticut River at Cornish, New Hampshire. Ice breakup occurred one week later. (Bottom) Looking across the river during brash ice motion at about 1 m/s. (Photos by M. Ferrick.)

For conversion of SI metric units to U.S./British customary units of measurement consult ASTM Standard E380-89a, *Standard Practice for Use of the International System of Units*, published by the American Society for Testing and Materials, 1916 Race St., Philadelphia, Pa. 19103.



**US Army Corps
of Engineers**

**Cold Regions Research &
Engineering Laboratory**

Kinematic Model of River Ice Motion During Dynamic Breakup

Michael G. Ferrick, Patricia B. Weyrick and David F. Nelson

September 1993

DTIC QUALITY INSPECTED 8

Accession For		
NTIS	CRA&I	<input checked="" type="checkbox"/>
DTIC	TAB	<input type="checkbox"/>
Unannounced		<input type="checkbox"/>
Justification		
By		
Distribution /		
Availability Codes		
Dist	Avail and/or Special	
A-1		

Prepared for
OFFICE OF THE CHIEF OF ENGINEERS

Approved for public release; distribution is unlimited.

PREFACE

This report was prepared by Michael G. Ferrick, Research Hydrologist, Patricia B. Weyrick, Physical Science Technician, and David F. Nelson, Physical Science Aid, Snow and Ice Branch, Research Division, U.S. Army Cold Regions Research and Engineering Laboratory, Hanover, New Hampshire.

Funding for this work was provided primarily by DA Project 4A162734DT08, *Combat Engineering Systems*, and also by DA Project 4A762784AT42, *Design, Construction and Operations Technology for Cold Regions*, Task CS, Work Unit 001, *River Ice Mechanics for Combat Engineering*.

The authors thank Jonas Eliasson, Mark Hopkins, Nathan Mulherin, Dr. Samuel Colbeck and an anonymous reviewer for comments on an earlier version of this manuscript. The authors also thank Edmund Wright for careful editing and Donna Harp for patiently preparing many drafts.

The contents of this report are not to be used for advertising or promotional purposes. Citation of brand names does not constitute an official endorsement or approval of the use of such commercial products.

CONTENTS

	Page
Preface	ii
Introduction	1
Kinematic model of ice motion	1
Ice continuity equation	2
Breaking front	3
Convergence front	4
Stoppage front	4
Release front	6
Ice discharge	6
1992 Connecticut River breakup data	7
Orthogonal polynomial fits to the data	7
Initial breaking front motion	11
Overall ice mass balance	11
Kinematic analysis of Connecticut River data	12
Event sequence	12
Ice and front motion	13
Conclusions	15
Literature cited	16
Abstract	17

ILLUSTRATIONS

Figure

1. Control volume with control surfaces 1 and 2 that either moves downstream or upstream with the corresponding front	2
2. Dimensionless breaking front speed as a function of relative river width times unit ice volume on either side of the front, and relative width times ice thickness for incoming sheet and selected values of accumulation porosity	3
3. Dimensionless ice convergence front speed as a function of relative river width times unit ice volume on either side of the front for a range of V_{i1}/V_{i2}	4
4. Steady motion and growth of an ice accumulation (shaded) depicted on the $x-t$ plane	5
5. Dimensionless ice stoppage front speed and dimensionless ice release front speed as a function of relative river width times unit ice volume on either side of the front	5
6. Ice stoppage occurring upstream of the breaking front depicted on the $x-t$ plane	6
7. Ice release at a point initiating breaking and release front motion depicted on the $x-t$ plane	7
8. Ice velocity data, best least-squares 7th and 12th order polynomial fits, and velocity error between the polynomials and the data for site D	8

9. Ice velocity data, best least-squares 7th and 11th order polynomial fits, and velocity error between the polynomials and the data for the first part of the motion at site U	9
10. Ice velocity data, best least-squares 7th and 15th order polynomial fits, and velocity error between the polynomials and the data for the second part of the motion at site U	10
11. Complete ice velocity data record for site U and best 11th and 15th order polynomials with a match point connecting them	10
12. Ice velocity and ice discharge upstream of the breaking and convergence fronts, and the celerity of the breaking front, for a range of accumulation unit volumes and initial convergence front speeds	14
13. Breaking and convergence front and ice particle motion on the $x-t$ plane that are most consistent with the Connecticut River data	15

TABLES

Table

1. Errors associated with polynomial fits to the ice velocity data	8
2. Parameters for a range of accumulation unit volume	12
3. Comparison of front speeds and positions for ranges of accumulation unit volume and initial convergence front speed	15

Kinematic Model of River Ice Motion During Dynamic Breakup

MICHAEL G. FERRICK, PATRICIA B. WEYRICK AND DAVID F. NELSON

INTRODUCTION

The process of dynamic ice breakup in a river is complex because of the interdependence of the water flow and the ice motion, and the rapid changes with time in both of these processes. The unsteady flow associated with dynamic breakup has been considered by several authors (e.g., Beltaos and Krishnappan 1982, Billfalk 1982, Doyle and Andres 1979, Ferrick and Mulherin 1989, Henderson and Gerard 1981, Prowse et al. 1986, Williamson 1989). However, in the static analyses of breakup ice jam formation of Beltaos (1988), Pariset et al. (1966) and Uzuner and Kennedy (1976), the flow and ice dynamics are neglected and jam formation is assumed to be independent of other breakup processes. The static force balance requires the ice to thicken in place by shoving and collapse until an equilibrium is reached between the internal strength of the accumulation and the steady hydraulic forces. Gerard and Flato (1988) emphasized the need for understanding the hydraulics and mechanics of moving ice accumulations and jam formation in the context of dynamic breakup. Recently Shen and Chen (1992) developed a dynamic model of flow and ice motion applied to the freezeup processes of a river, and Guo (1991) proposed a dynamic model of ice breakup.

A first step in describing many river ice and flow processes is the conservation of mass. Lighthill and Whitham (1955) used continuity to develop a kinematic wave model of traffic flow on crowded roads. When congested traffic ahead is slower than that behind, these waves coalesce into a "shock wave" or front that causes rapid speed reduction of vehicles upon arrival. Risebro and Tveito (1992) presented a front tracking method for solving hyperbolic conservation laws. The solution is represented by an arbitrary number of piecewise constant states separated by discontinuities or fronts. These fronts are shock

or rarefaction waves, whose motion is tracked in the $x-t$ plane until they interact.

In this report we obtain simultaneous ice velocity records with time at a pair of sites bounding a reach of the Connecticut River from fixed video cameras and orthogonal target grids (Ferrick et al. 1992). The ice motion at the sites differed, raising questions that include how these views of the motion are related, and whether the data obtained at two points can be used to understand the ice dynamics of the reach. An analogy is proposed between the ice motion during dynamic breakup and the flow of traffic on crowded roads. We then develop a kinematic model of river ice motion from the continuity equation and identify several fronts in the ice. The fronts are tracked in the $x-t$ plane to obtain a hypothetical event sequence and to describe the ice motion in the reach from the data. The resulting ice accumulation forms while the breakup is in progress. The dynamic tracking of ice particles and fronts with jamming as an integral part of breakup replaces the usual assumption of static jam formation.

KINEMATIC MODEL OF ICE MOTION

To construct our model, we will visualize the existence of different "fronts" that move through the ice field in response to changing conditions. The *breaking front* travels downstream and separates the stationary ice ahead from the moving ice behind. The *convergence front* moves with the upstream limit of an ice accumulation, delineating it from thinner ice upstream. Analogies for these fronts occur at both ends of a congested traffic accumulation moving at a reduced speed. Additional vehicles regularly added to the front of the accumulation cause the breaking front to travel faster than the group. Behind the group

at the convergence front, faster moving vehicles slow to the group speed and become part of the accumulation. The *stoppage front* travels upstream following the arrest of ice motion, and separates the moving ice upstream from ice at rest downstream. The *release front* moves upstream through the ice field, initiating motion in response to an ice release downstream. A red light interrupts a traffic flow, causing vehicles to stop in response to those ahead. The stoppage front progresses "upstream" at a rate dependent on vehicle separation. Following a green light, vehicle motion is initiated in response to that ahead, and this release front also travels "upstream."

Ice continuity equation

The conservation of mass can be written for the ice near each front that relates the speed of the front to the change in ice thickness and accumulation porosity across the front. The ice discharge on either side of each front can also be obtained. Ice continuity equates the time rate of change of mass in an arbitrary control volume (CV) to the net efflux of mass across the control surface. We will use the CV de-

picted in Figure 1, containing and moving with a front at speed C in the downstream direction. Ice does not accumulate in this moving CV and there is no time rate of change term to consider. Ice moving at velocity V_{i1} enters the control volume through downstream control surface 1, and an equal quantity exits the control volume through upstream surface 2 at V_{i2} . The relative velocities between the ice and the upstream and downstream control surfaces are $C - V_{i2}$ and $C - V_{i1}$, respectively. The areas of the control surfaces are Bt_i , where B is the river width, and t_i is the thickness of the ice sheet or accumulation. The ice continuity equation then states the flux balance as

$$B_1 (C - V_{i1}) t_{i1} (1 - e_{c1}) = B_2 (C - V_{i2}) t_{i2} (1 - e_{c2}) \quad (1)$$

where e_c is the porosity of the ice accumulation. We refer to the ice volume per unit surface area, $t_i (1 - e_c)$, as the unit ice volume. The general form of eq 1 is

$$(C - V_{i1}) = R(C - V_{i2}) \quad (2)$$

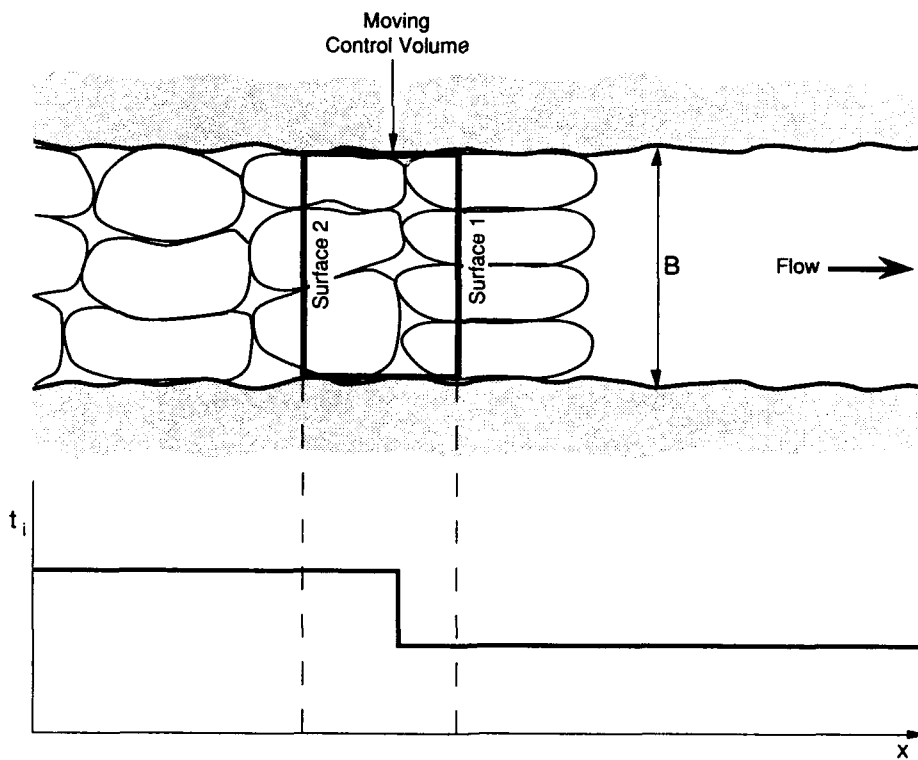


Figure 1. Control volume with control surfaces 1 and 2 that either moves downstream or upstream with the corresponding front. An abrupt parameter transition at a front between constant states on each side of the CV is shown for ice thickness.

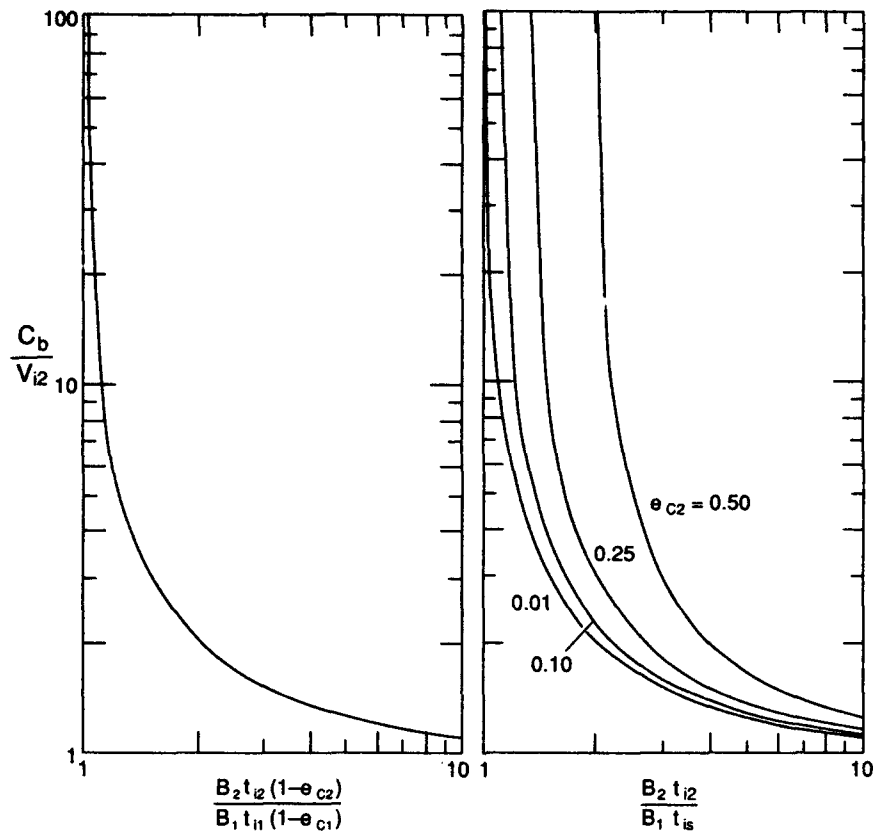


Figure 2. Dimensionless breaking front speed as a function of (left) relative river width times unit ice volume on either side of the front, and (right) relative width times ice thickness for incoming sheet and selected values of accumulation porosity.

where R represents the dimensionless ratio of effective control surface areas as

$$R = \frac{B_2 t_{i2} (1 - e_{c2})}{B_1 t_{i1} (1 - e_{c1})} \quad (3)$$

In the development of eq 2 the CV was assumed to move in the downstream direction. This sign convention yields negative speed $-C$ for fronts moving upstream.

Breaking front

We will first consider a reach of broken ice that has jammed upstream of an intact ice cover. A flow surge traveling downstream arrives at the accumulation, and at some point ice motion is initiated. Downstream ice movement continually adds material to the front of the moving pack, and the speed of the breaking front C_b is always greater than the local ice velocity V_{i2} . With appropriate substitutions, the dimensionless breaking front speed can be obtained from eq 2 as

$$\frac{C_b}{V_{i2}} = \frac{R_b}{R_b - 1} \quad (4)$$

with R at the breaking front, $R_b \geq 1$. If the breaking front encounters an unbroken ice sheet of thickness t_{is} instead of ice rubble, $t_{i1} = t_{is}$ and if there is negligible open water area in the sheet, the incoming sheet "porosity" $e_{c1} = 0$.

The movement of a breaking front causes ice convergence, which results in a decreased surface area occupied by the ice. The relationship between dimensionless breaking front speed and relative river width times unit ice volume given by eq 4 is depicted in Figure 2. Significant changes in river width do not usually occur in a longitudinal distance of less than one river width. When the ice passing through the control volume thickens substantially or the porosity of the accumulation decreases greatly, the breaking front speed is only marginally higher than the ice velocity. However, as the ratio of unit ice volumes across the front approaches 1, the breaking front celerity becomes large. Figure 2 also presents the dimensionless breaking front speed of advance into an

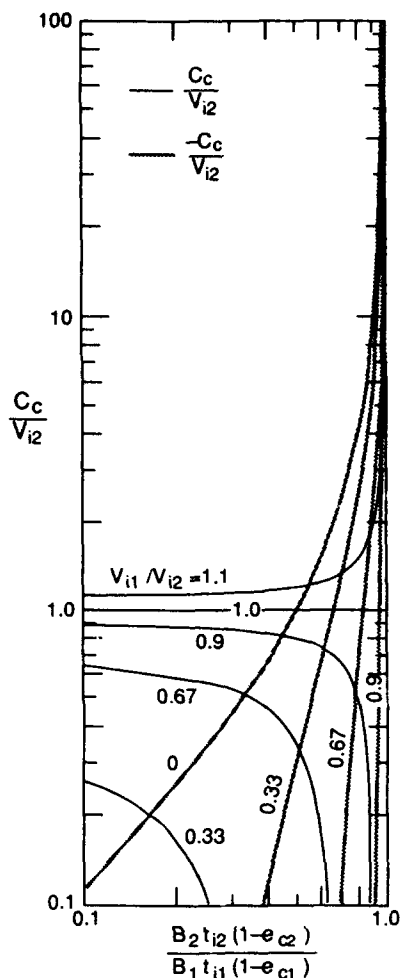


Figure 3. Dimensionless ice convergence front speed as a function of relative river width times unit ice volume on either side of the front for a range of V_{i1}/V_{i2} . Negative or upstream speeds are distinguished from positive downstream speeds.

intact, stationary ice sheet, as a function of the accumulation to sheet thickness ratio for a range of accumulation porosities. The thickness ratio at which the breaking front speed becomes very large depends on the porosity of the accumulation. For larger thickness ratios this speed is small for all porosities.

Convergence front

In the ice accumulation immediately upstream of the breaking front the total resistance to motion is relatively high. Farther upstream, the motion resistance is lower and higher ice velocities are typical. This velocity difference causes ice convergence at the upstream limit of a moving accumulation. For sim-

plicity we visualize this accumulation as a rigid body with a uniform velocity. All ice convergence occurs at the convergence front, located at the upstream limit of the accumulation. Consider a CV that moves with the convergence front at the head of the accumulation at speed C_c . The control surface designations are those of Figure 1, and the dimensionless speed of the ice convergence front is obtained from eq 2 as

$$\frac{C_c}{V_{i2}} = \frac{V_{i1} - R_c}{1 - R_c} \quad (5)$$

where V_{i1} is the accumulation velocity, V_{i2} is the velocity of the ice immediately upstream, $R_c < 1$ indicates convergence of thinner or more porous ice from upstream of the accumulation, and C_c is positive for downstream front motion or negative for fronts moving upstream. The dimensionless convergence front speed is given in Figure 3 as a function of R_c for a range of ice velocity ratios. Ice accumulations upstream of a relatively slow moving breaking front would generally have velocity ratios of less than 1. Then, as the speed of the accumulation decreases, the convergence front speed also decreases or becomes more negative for all R_c values. This front speed also decreases or becomes more negative as R_c increases for all velocity ratios. However, divergence and shortening at the upstream limit of the accumulation are indicated by dimensionless front speeds greater than 1, and the front speed increases with both R_c and the velocity ratio.

The growth of an ice accumulation during a period of steady motion is shown on the $x-t$ plane in Figure 4. Paths of front motion and selected ice motion are displayed in time and space on this plane. Stationary ice initially downstream of the breaking front is incorporated into the accumulation as the front passes. Ice initially upstream of the convergence front overtakes it and is also incorporated into the accumulation. The total length of the accumulation is the x -distance between these fronts. Both the breaking and convergence fronts deflect the path lines tracing the ice motion. The parallel path lines between the fronts reflect assumed rigid body motion of the accumulation.

Stoppage front

A continuity equation can be written for the stoppage of ice motion that progresses upstream following the arrest of a breaking front or of the moving ice somewhere behind this front. In this case the CV depicted in Figure 1 moves upstream at speed C_s with the stoppage of ice motion. Moving ice enters

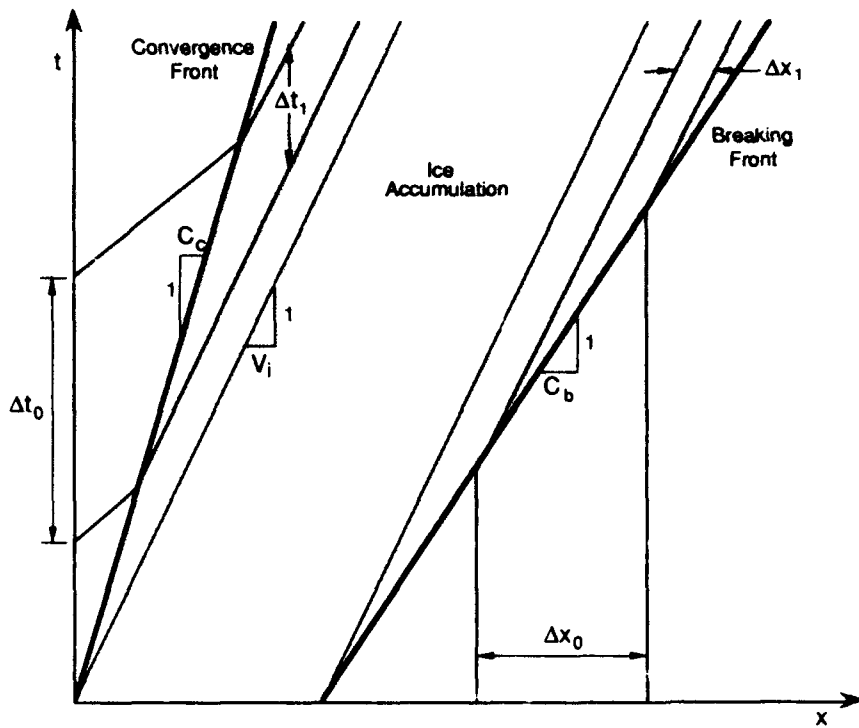


Figure 4. Steady motion and growth of an ice accumulation (shaded) depicted on the $x-t$ plane. The spatial and temporal separation of ice particles is reduced upon entering the accumulation and constant thereafter.

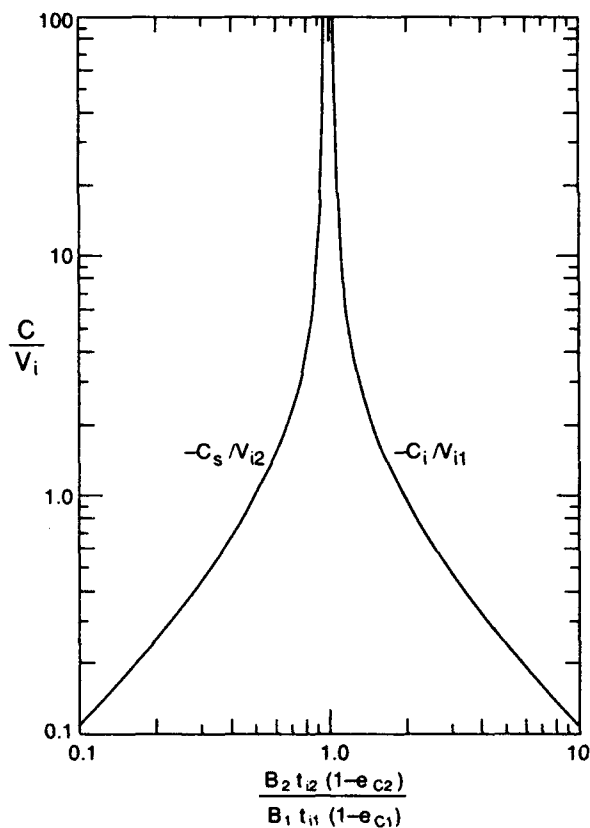


Figure 5. Dimensionless ice stoppage front speed and dimensionless ice release front speed (upstream) as a function of relative river width times unit ice volume on either side of the front.

through the upstream control surface and exits through the downstream surface as stationary ice. Solving eq 2 for the dimensionless speed of the ice stoppage front yields

$$\frac{C_s}{V_{i2}} = \frac{-R_s}{1-R_s} \quad (6)$$

with $R_s \leq 1$, indicating the unit ice volume downstream of the front is greater than that upstream. Therefore, packing during an ice stoppage is limited by the downstream unit ice volume that cannot be exceeded. Low stoppage front speeds in Figure 5 reflect significant packing during ice arrest, but as R_s approaches 1, the front progresses upstream very rapidly. The breaking and stoppage fronts are opposites, and their continuity equations have the same form. The distinction is the inverse relationship between the unit ice volume across each front.

A stoppage front is the limiting case of a convergence front with a velocity ratio of zero. As the speed of an ice accumulation approaches zero, C_c becomes negative, the convergence front becomes a stoppage front, and eq 5 reduces to eq 6. An ice stoppage is illustrated on the $x-t$ plane in Figure 6. The initial stoppage occurs upstream of the breaking front, and the stoppage front travels upstream instantaneously through the rigid body accumulation. The stoppage and convergence fronts merge into a single front at the upstream limit of the accumulation. Then, the

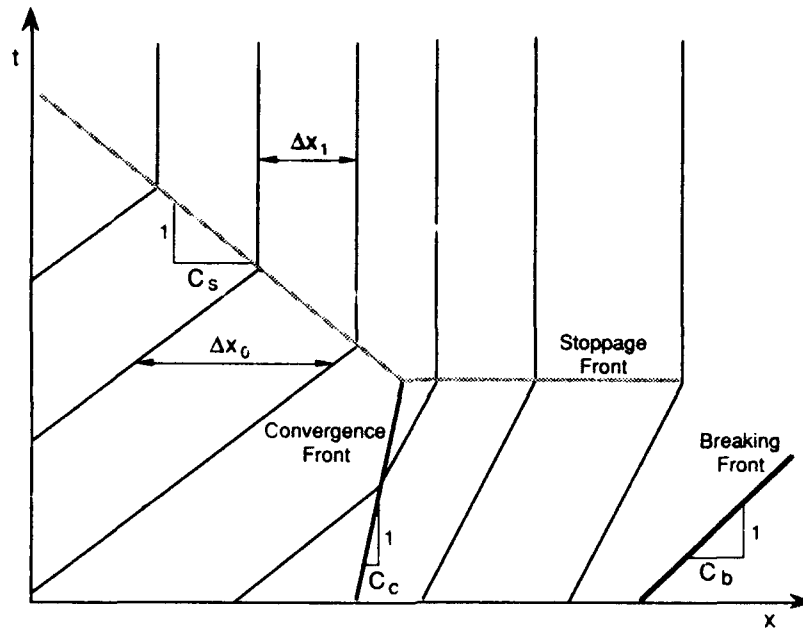


Figure 6. Ice stoppage occurring upstream of the breaking front depicted on the $x-t$ plane. The path lines show reduced spatial separation of ice particles upstream of the accumulation following passage of the stoppage front.

stoppage front continues upstream at speed C_s , bringing that ice to a halt.

Release front

We can also write a continuity equation for a failure of the resistance at a point and the initiation of ice motion. In this case the CV shown in Figure 1 moves upstream at a speed C_i with the release of the ice and initial motion. Stationary ice enters through the upstream control surface, and exits through the downstream surface as moving ice. The dimensionless speed of the ice release front is obtained from eq 2 as

$$\frac{C_i}{V_{i1}} = \frac{-1}{R_i - 1} \quad (7)$$

with $R_i \geq 1$. Ice release causes divergence, as the water surface area available to an ice accumulation is increased. The dimensionless speed of the ice release front is depicted in Figure 5. With $R_i \approx 1$ ice divergence is small, approximating rigid body motion, and the front speed is very large. However, as R_i increases, indicating substantial divergence, the dimensionless release front speed approaches zero. An ice release is depicted on the $x-t$ plane in Figure 7. A breaking front travels downstream and a release front travels upstream from the point of the release.

Both fronts initiate ice motion, with convergence occurring upstream of a breaking front and divergence occurring downstream of a release front.

Ice discharge

The ice discharge at point p Q_p can be written as

$$Q_p = B_p V_{ip} t_{ip} (1 - e_{cp}) \quad (8)$$

Each of the continuity equations associated with front motion can be solved to obtain the ice discharge near the front. The ice discharge upstream of the breaking front Q_b is obtained from eq 4 and 8 as

$$Q_b = C_b D_b \quad (9)$$

where

$$D = B_2 t_{i2} (1 - e_{c2}) - B_1 t_{i1} (1 - e_{c1}) \quad (10)$$

and D_b is the value of D associated with the breaking front. The ice discharge upstream of the convergence front Q_c can be obtained from eq 5 and 8 as

$$Q_c - Q_b = C_c D_c \quad (11)$$

The ice discharge upstream of the stoppage front Q_s can be obtained from eq 6 and 8 as

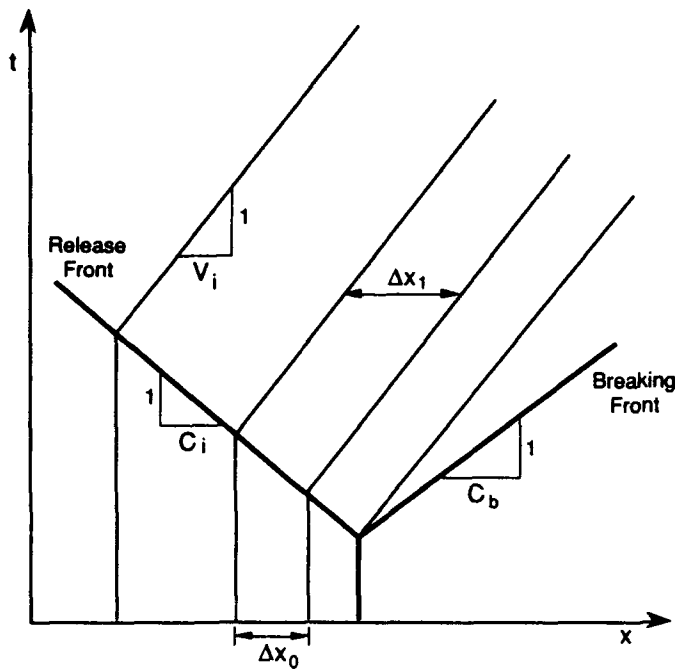


Figure 7. Ice release at a point initiating breaking and release front motion depicted on the $x-t$ plane. The path lines show increased spatial separation of ice particles following passage of the release front.

$$Q_s = -C_s D_s \quad (12)$$

Finally, the ice discharge downstream of a release front Q_i is obtained from eq 7 and 8 as

$$Q_i = C_i D_i \quad (13)$$

1992 CONNECTICUT RIVER BREAKUP DATA

Breakup of the Connecticut River ice cover near Windsor, Vermont, occurred on 11 March 1992. Prior to breakup we installed an orthogonal grid of video targets with known dimensions at two sites, separated by a 1600-m reach. The upstream site was designated site U and the downstream site was D. Tripod-mounted video cameras were positioned at the top of the river bank to record the motion of the ice through the grid at each location. The cameras remained focused on the original grid location for the entire period of motion, and audio marks on each videotape were used to synchronize the times. Each videotape was window dubbed with continuous on-screen digital time accurate to ± 0.03 s. Points on the ice to be used for velocity measurement were chosen by their contrast from the surrounding ice. The grid scale divided by the travel time provides an ice velocity estimate at the mean time of the interval. The breakup occurred in two ice movements, separated

by about 3 hours during a period of increasing discharge. In this report we will analyze the initial period of ice motion and use data from the second motion for hypothesis testing.

Orthogonal polynomial fits to the data

The methods described by Ferrick et al. (1992) were used to obtain least-squares orthogonal polynomial fits to the ice velocity data. The polynomials are used to quantify the variability in the data for comparison with expected measurement error and to verify that velocity variations across the channel can be neglected. The length of ice passing between specified times and the ice acceleration at a given time are obtained by integration and differentiation, respectively, of the corresponding polynomial. Accurate estimates of ice acceleration cannot be obtained from the raw data. Polynomials of increasing degree incorporate additional information from the data until the magnitude of the maximum error ceases to decrease and the structure of the error is random. A polynomial of appropriate order can be found by observing both the absolute magnitude and randomness of the error. The 7th- and 12th-order polynomials are presented together with the data from site D in Figure 8. The 7th-order polynomial represents the highest order for which a composite polynomial equation is available. The errors between these polynomials and the data are also given in Fig-

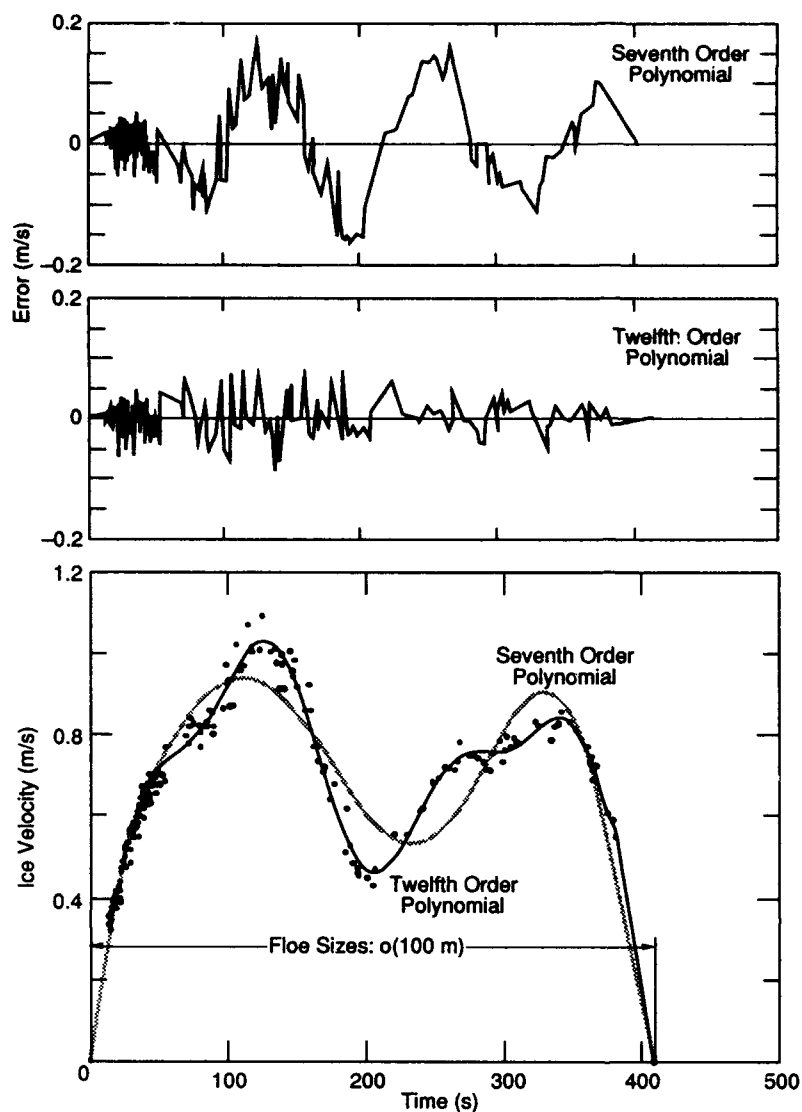


Figure 8. Ice velocity data, best least-squares 7th and 12th order polynomial fits, and velocity error between the polynomials and the data for site D. The predominant floe size during this ice motion was on the order of 100 m.

Table 1: Errors associated with polynomial fits to the ice velocity data.

Site	Polynomial degree	Maximum polynomial ice velocity (m/s)	Maximum measurement error (m/s)	Maximum error (polynomial-data) (m/s)	Mean polynomial ice velocity (m/s)	Measurement error at mean velocity (m/s)	RMS error (polynomial-data) (m/s)
Upstream 0-420s	7	1.36	0.109	0.113	0.89	0.065	0.039
	11	1.34	0.107	0.095			
Upstream 420-970s	7	2.37	0.222	0.429	1.24	0.097	0.083
	15	2.34	0.218	0.194			
Downstream 0-420s	7	0.93	0.069	0.165	0.66	0.047	0.064
	12	1.02	0.077	0.089			

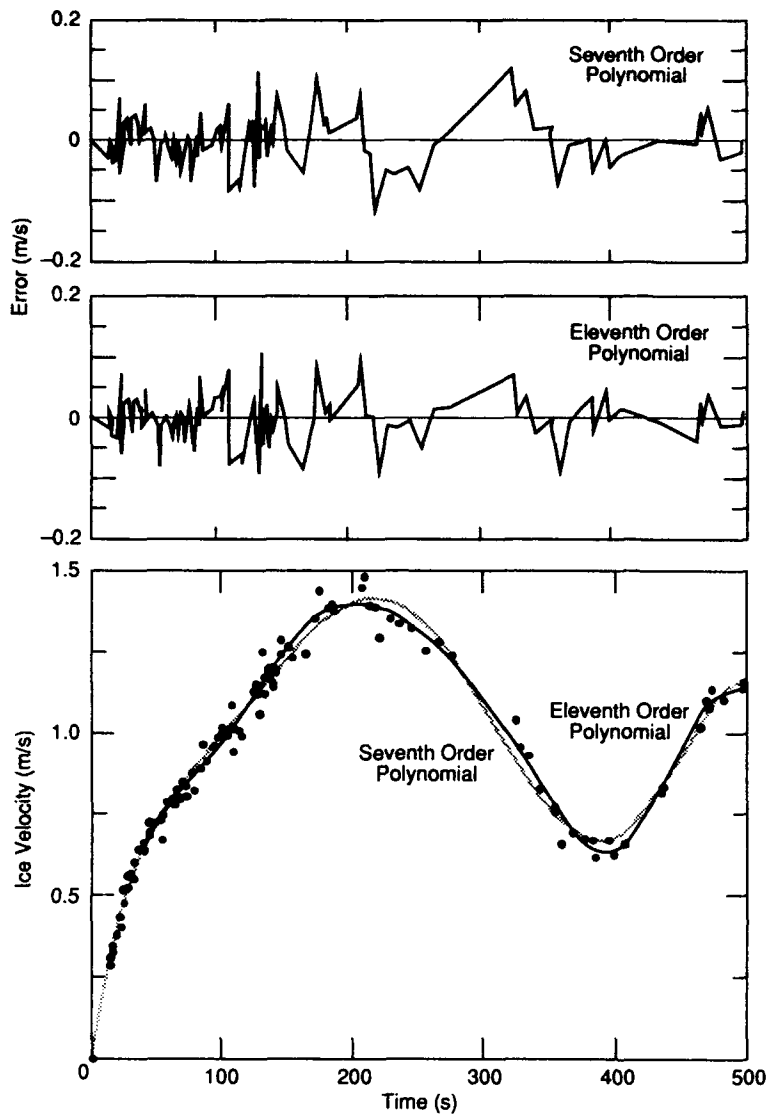


Figure 9. Ice velocity data, best least-squares 7th and 11th order polynomial fits, and velocity error between the polynomials and the data for the first part of the motion at site U.

ure 8. The 7th-order error has structure, and is larger in magnitude than the 12th-order error. Figure 9 presents the data, polynomials, and errors for the first part of the longer record at site U, and Figure 10 gives comparable information for the second part of this record. The order of the polynomial providing the best least-squares fit depends on the length and complexity of the data record. The best polynomials for each time segment were obtained by assuming a match point at a common time. We present the complete data record for site U and a continuous polynomial representation of ice velocity in Figure 11.

Maximum measurement errors in obtaining data from the videotape were 1.0 m in length and 0.2 s in elapsed time. These estimates were obtained from known target size and width of grid lines superposed

on the videotape, and the precision of viewing a target-line intersection. When these errors are combined unfavorably the error in the computed ice velocity increases with the ice velocity. A maximum error of 0.08 m/s at an ice velocity of 1 m/s increases to 0.23 m/s at a velocity of 2.5 m/s. Ice velocity errors between the various polynomials and the data are compared with measurement errors in Table 1. The maximum polynomial-data errors are slightly less than the maximum measurement errors for the upstream site, and slightly greater for the downstream site. The RMS polynomial-data errors average only 57% of the maximum measurement error at the mean velocity and 32% of the overall maximum measurement error. Therefore, most of the error in the ice velocity polynomials (Fig. 8, 9, 10) can be attributed to mea-

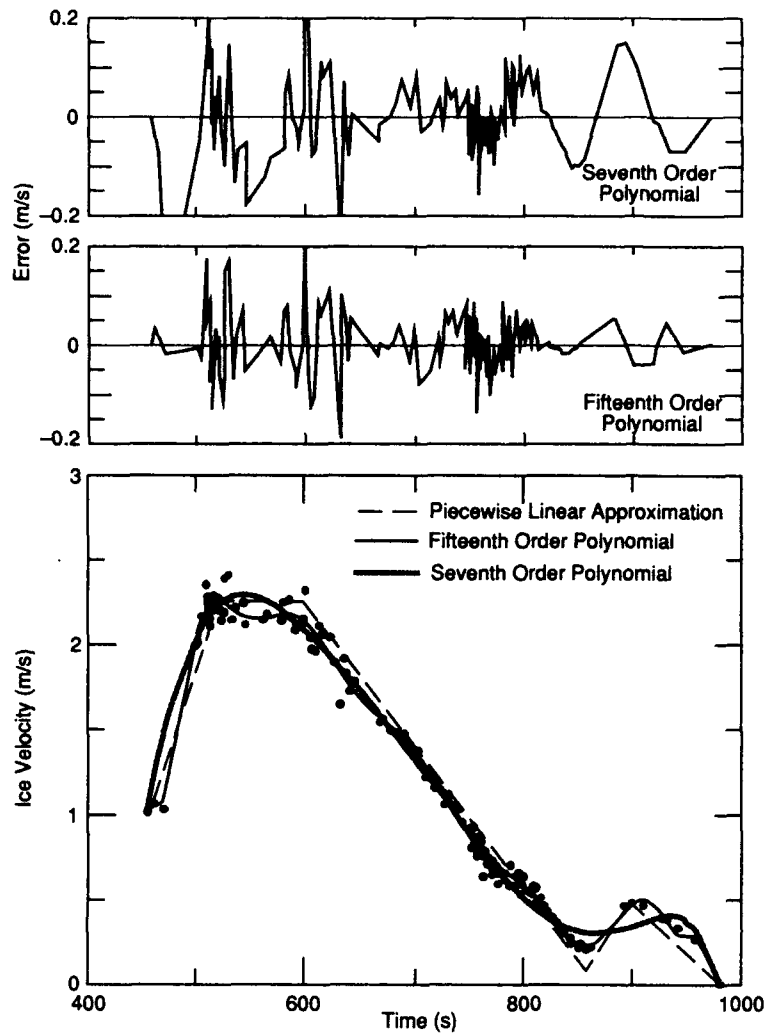


Figure 10. Ice velocity data, best least-squares 7th and 15th order polynomial fits, and velocity error between the polynomials and the data for the second part of the motion at site U. A piecewise linear ice velocity for the motion calculations is also shown.

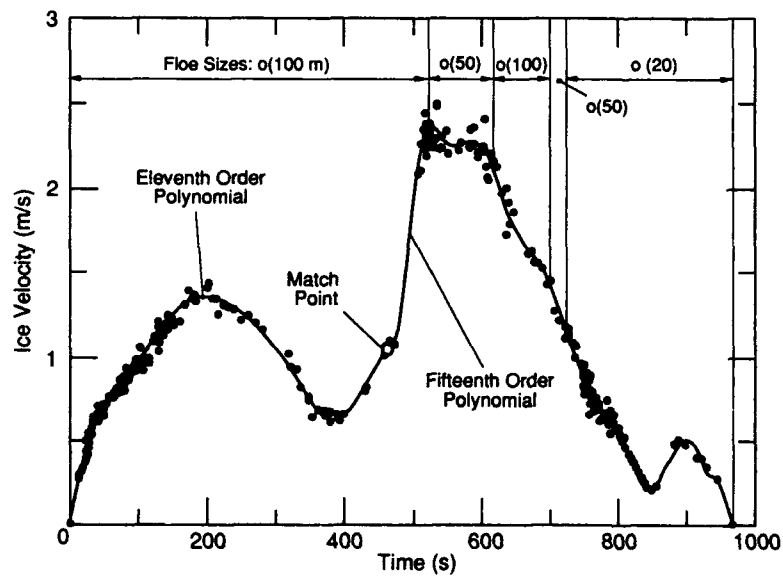


Figure 11. Complete ice velocity data record for site U and best 11th and 15th order polynomials with a match point connecting them. The predominant floe size is indicated as a function of time.

surement error, and these polynomials represent the ice velocity as well as the data. There is no evidence of significant velocity differences across the channel.

Initial breaking front motion

The river discharge prior to ice motion was 980 m³/s and gradually increased. The initial ice movement was the result of a support breakup of the river reach. The bank support failed and the ice sheet moved as a large plate with minimal convergence and rubble formation. Other characteristics of support breakup are given by Ferrick and Mulherin (1989). The ice near the banks at the downstream site failed almost continuously during the ice motion. The ice acceleration calculated for each site using the velocity polynomial was within 3% of 0.0266 m/s² following breaking front arrival. At 50 s the ice velocities were equal at the sites, an indicator of nearly rigid plate initial motion. The time lag between initial ice motion at the two camera sites was only 2 s, indicating a breaking front speed of 800 m/s in the downstream direction. With C_b/V_i very large, the moving control volume analysis indicates that the ice sheet was unchanged as the breaking front passed through the reach except that motion was initiated. This result concurs with the analysis of Ferrick et al. (1992) that ice upstream of a rapidly moving breaking front moves almost as a rigid body. The fast breaking front speed also supports the modeling concepts of force balance per unit length and instantaneous support breakup of a reach (Ferrick and Mulherin 1989).

Water fountaining above the level of the ice, possibly indicating a pressure flow, was not observed near either site. The ice cover was cracked continuously along both banks, and moved readily in the vertical direction in response to changing water levels. Therefore, the rapid front motion was not caused by pressure waves in the flow. Bourbie et al. (1987) present pressure wave speed V_p for an isotropic material as

$$V_p = \left[\frac{E(1-\nu)}{\rho(1+\nu)(1-2\nu)} \right]^{1/2} \quad (14)$$

where E is the elastic modulus, ν is Poisson's ratio, and ρ is density. The pressure wave speed in fresh-water ice at its melting point varies between 3700 m/s for intact ice and 2000 m/s for deteriorated ice. The most likely cause of the rapid front motion was pressure transmitted downstream through the ice, interrupted and slowed occasionally by ice failure.

Overall ice mass balance

The length of ice sheet that passed each site during this ice motion can be found by integrating the ice velocity polynomials. The quantity of ice that accumulated in the reach A_q between times t_0 and t_1 can then be obtained as

$$A_q = B_u \int_{t_0}^{t_1} V_{iu} t_{iu} (1 - e_{cu}) dt - B_d \int_{t_0}^{t_1} V_{id} t_{id} (1 - e_{cd}) dt \quad (15)$$

where subscripts u and d indicate sites U and D , respectively. The river width at site U , B_u is 140 m, and the width at site D , B_d is 135 m. The length of ice rubble in the reach L_r is measured downstream from site U to the breaking front. The final rubble accumulation contains the net ice accumulation in the reach during the motion and the additional rubble that was generated in the reach at the breaking front and the convergence front

$$L_r t_{ir} (1 - e_{cr}) = L_r t_{is} + A_q / \bar{B} \quad (16)$$

where the average width of the river in the accumulation reach, \bar{B} is 190 m and the subscript r indicates parameters of the rubble. Solving eq 16 for the length of the rubble reach we obtain

$$L_r = \frac{A_q / \bar{B}}{t_{ir} (1 - e_{cr}) - t_{is}} \quad (17)$$

Then, the volume of ice rubble in the final accumulation A_v is obtained as

$$A_v = \bar{B} t_{ir} (1 - e_{cr}) L_r \quad (18)$$

Beltaos (1988) and Calkins (1978) reported extensive ice jam thickness measurements. The thickness was generally greatest near the toe and decreased with distance upstream. However, in all cases the mean cross-sectional thicknesses were nearly constant over much of the jam length. The mean thickness of these jams ranged from 2 to 5 times the original sheet thickness. The ice in the reach between the camera sites is idealized as having two components: ice plates with a unit volume comparable to the origi-

Table 2: Parameters for a range of accumulation unit volume.

$t_{ir}(1-e_{cr})$ (m)	L_{r0} (m)	L_r (m)	Percent of reach as rubble	A_v ($m^3 \times 10^{-3}$)	R_b	C_b/V_{ib}
0.75	120	1100	69	157	1.5	3.0
0.83	90	840	53	133	1.67	2.5
1.00	60	570	36	108	2.0	2.0
1.10	50	480	30	100	2.2	1.83
1.20	43	410	26	94	2.4	1.71
1.25	40	390	24	93	2.5	1.67
1.30	38	370	23	91	2.6	1.63
1.40	33	330	21	88	2.8	1.56
1.50	30	300	19	86	3.0	1.5

nal sheet, and rubble with a greater unit volume. For simplicity and consistency with observations, we assume the rubble accumulation to have uniform thickness and porosity, and consider a range of unit ice volumes $t_{ir}(1 - e_{cr})$ from 0.75 m to 1.5 m, for an original sheet thickness t_{is} of 0.5 m.

Ice rubble was not observed near site D during or after the ice motion, except for minor accumulations along the banks. Prior to 700 s the moving ice at site U was also large plates or a continuous sheet with an undisturbed unit volume of 0.5 m. The quantity of ice accumulating in the reach between the initial motion and 460 s was obtained from eq 15. We assume that half of this total resides in the primary accumulation, and calculate its initial length L_{r0} from eq 17 as a function of unit ice volume. All of the ice entering the reach after 460 s is assumed to be part of this accumulation. Between 700 and 860 s the ice passing site U was more broken and concentrated, and we estimate the unit volume at 0.66 m. At 860 s the convergence front arrived at site U, and the unit volume was that of the accumulation. With these data the final accumulation length L_r can be found from eq 17 for each assumed unit ice volume. The parameters R_b and C_b/V_i are obtained for each unit volume from eq 3 and 4, and all these results are summarized in Table 2. The dimensionless breaking front speed, and the length and volume of the rubble vary significantly with the assumed unit ice volume.

Three hours after initial ice motion a second support breakup was recorded by the video camera at site D. This videotape indicated that most of the ice rubble in the reach was in the primary accumulation, and was the basis for that assumption. Ice velocity data were obtained and polynomials were fitted to these data. Integration of the polynomials provided length scales that were used to obtain an estimate of the length of the earlier ice accumulation between the camera sites. The river at the downstream site is narrower than in the reach between the sites. Cor-

recting for the difference in width we obtain an initial accumulation front location 1110 m upstream and an initial accumulation length of about 490 m. Table 2 indicates close agreement of this length with that for a unit ice volume of 1.10 m. During this second ice release about 1 km of ice sheet and 8 km of rubble moved by the downstream site at an average speed of almost 3 m/s. With the 1.1 accumulation unit volume used in eq 8 we obtain an average ice discharge of about 450 m^3/s .

KINEMATIC ANALYSIS OF CONNECTICUT RIVER DATA

Event sequence

We will now develop an event sequence from the data with the ice continuity equations in order to learn as much as possible about the dynamics of the 1992 Connecticut River breakup. Throughout the initial 420 s of motion, the ice moved as large plates or sheets at both sites (Fig. 8, 9). The arrest of the motion at site D at 420 s initiated a stoppage front that traveled upstream. This front arrived 555 s later at site U, corresponding to an average speed of only 2.9 m/s. With this front speed and an average ice velocity of about 1 m/s (Fig. 10), the downstream ice must initially have a much greater unit volume than that upstream (Fig. 5). However, all ice visible from site D was a uniform sheet, indicating that a single stoppage front is not consistent with the data and observations. The abrupt increase in ice velocity at site U after 460 s corresponds to a rapid decrease in the local resistance to motion. The initiation of a breaking front downstream would generate this response. Therefore, we will assume that the stoppage front traveled rapidly upstream to a location near site U in about $460 - 420 = 40$ s. The average front speed of 35 m/s requires negligibly thicker ice downstream and minimal convergence would have occurred. At

460 s the stoppage front stalled and then began moving downstream as a second breaking front. The ice accumulation upstream of the breaking front was thicker and had a greater unit volume than the stationary plates downstream. The convergence front arrived at site U from downstream at 860 s. Prior to that time the ice velocity decreased almost linearly without noticeable convergence. If site U was typical of nearby locations, the steady unit ice volume indicates rapid, rigid-body response to changes in the motion downstream. We hypothesize that after 460 s the front and ice motions in the reach downstream are reflected in the observations and velocity measurements at site U, and that the regions of ice convergence are limited to the fronts. For these conditions the kinematic model indicates that the breaking front moved continuously, stalled briefly, moved again, and finally arrested. The ice in the accumulation mimicked this behavior. While the breaking front was moving downstream the convergence front moved upstream, and the accumulation lengthened rapidly. The convergence front gradually became a stoppage front as the breaking front speed and accumulation ice velocity decreased.

Ice and front motion

We will now calculate the ice and front motion downstream of site U from 460 s until the motion arrests at 975 s. For simplicity the piecewise linear approximation of the ice velocity shown in Figure 10 will be taken as V_{iu} . The quantity of ice obtained from eq 15 and the linear approximation is within 1% of that using the polynomial for a wide range of accumulation unit volumes. The assumed rigid body motion of the ice between site U and that just upstream of the convergence front relates V_{ic} to V_{iu} by the relative river widths

$$V_{ic} = \frac{B_u V_{iu}}{B} \quad (19)$$

and $V_{ic} = V_{i2}$ of the CV at the convergence front. The ice accumulation behind the breaking front is also assumed to be rigid with uniform thickness, porosity and speed, and the ice velocity upstream of the breaking front $V_{ib} = V_{i1}$ of the CV at the convergence front. The rigid body assumptions limit the ice convergence to the breaking and convergence fronts.

Measured ice velocities on either side of the convergence front together with known unit ice volumes in eq 5 yield the time variable front speed. However, here we have only a single velocity measurement and must assume an average convergence front speed in order to calculate the ice velocity on the other side of the front. The corresponding ice discharges can then

be obtained with eq 4, 9 and 11. Parameter ranges will be used to assess the sensitivity of the calculations to unit ice volume of the accumulation (0.83, 1.1, 1.4 m) and initial average convergence front speed (-0.3, -0.1, 0.1 m/s). This speed is taken as a constant until a change occurs in the unit ice volume arriving at the front from upstream. We assume that this change should not affect the speed of the breaking front. The ratio of the ice velocities on either side of the convergence front is set equal to that from the previous time step, and C_c is recomputed using eq 5. This assumption can be visualized in Figure 3 as a change in the ratio of unit ice volumes along a line of constant V_{ib}/V_{ic} , providing a new C_c/V_{ic} . Afterward, C_c is again held constant and ice velocity is computed until the next change in unit volume of incoming ice. With the time of convergence front arrival at site U, C_c and L_{ro} known, the initial breaking and convergence front positions can be determined. Then, the front positions and all ice particle positions between sites U and D can be determined through time.

Ice velocity and ice discharge upstream of the breaking and convergence fronts, and celerity of the breaking front are presented in Figure 12 for ranges of accumulation unit volume and initial convergence front speed. The zero time in Figure 12 corresponds to an event time of 460 s. The ice accumulation velocity V_{ib} increases as its unit volume decreases and as the initial front speed increases. V_{ib} is obtained directly from the measurements after 400 s (860 s event time), and does not vary with these parameters. The ice velocity upstream of the convergence front V_{ic} , obtained from eq 19 and the measured data, was always greater than V_{ib} prior to 400 s and unknown afterward. The ratio $V_{ib}/V_{ic} < 1$ indicates ice convergence at the upstream end of the accumulation over the assumed parameter ranges. The trends in breaking front celerity follow those of the ice velocity. The exception is after 400 s when C_b increases with decreasing accumulation unit volume, while V_{ib} does not have this dependence. The ice discharge of the accumulation upstream of the breaking front Q_b increases slightly as the accumulation unit volume decreases, and increases more significantly as the initial convergence front speed increases. After 400 s Q_b varies only with the unit volume and displays the opposite trend. The ice discharge upstream of the convergence front Q_c does not vary over the parameter ranges. Differences in Q_c result from the variable arrival times of thicker ice from upstream at the convergence front. Q_c is always greater than Q_b except when C_c is positive.

A comparison of front speeds and positions is

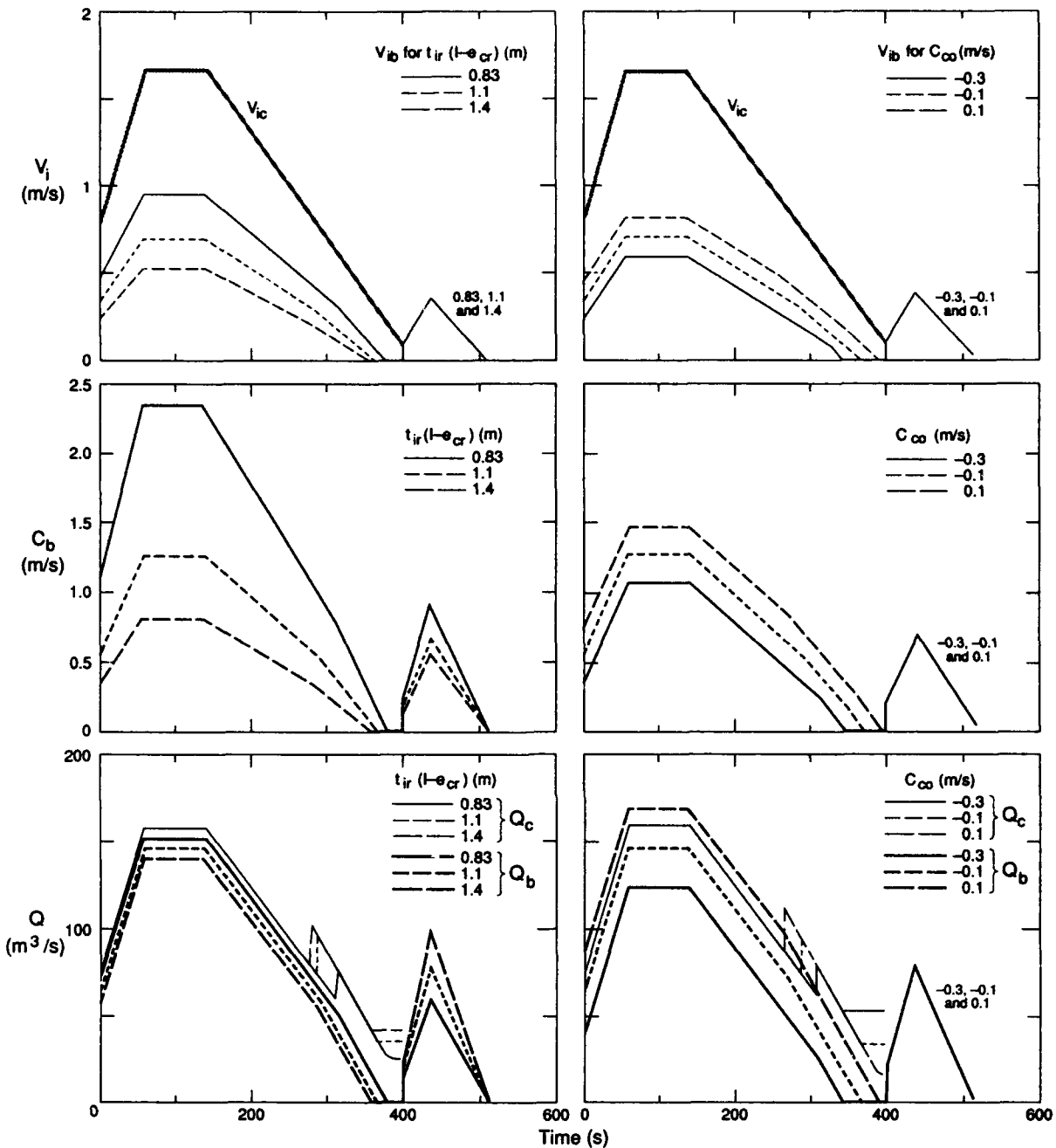


Figure 12. Ice velocity and ice discharge upstream of the breaking and convergence fronts, and the celerity of the breaking front, for a range of accumulation unit volumes and initial convergence front speeds.

given in Table 3 for the assumed parameter ranges. The initial convergence and breaking front positions X_{co} , X_{bo} were always near site U at $x = 0$ with a total range of 150 m. The intersection time of the thicker ice from upstream with the convergence front increased with decreasing convergence front speed and accumulation unit volume, having a total range of 50 s. The change in convergence front speed follow-

ing the intersection ΔC_c decreased with increasing unit volume, but was insensitive to initial convergence front speed. The total distance traveled by the breaking front ΔX_b and the average breaking front speed C_b increased with convergence front speed and with decreasing unit volume of the accumulation. The positions of the breaking and convergence fronts and several ice particles are traced through time on

Table 3: Comparison of front speeds and positions for ranges of accumulation unit volume and initial convergence front speed.

$t_{ir}(1-e_{cr})$ (m)	C_{c0} (m/s)	Intersection		ΔC_c (m/s)	X_{c0} (m)	X_{b0} (m)	ΔX_b (m)	\bar{C}_b (m/s)
		time (s)						
1.1	-0.3	309		-0.33	149	199	285	0.55
1.1	-0.1	290		-0.30	73	123	355	0.69
1.1	+0.1	266		-0.29	-2	48	426	0.83
0.83	-0.1	315		-0.62	93	183	654	1.27
1.1	-0.1	290		-0.30	73	123	355	0.69
1.4	-0.1	278		-0.19	63	96	231	0.45

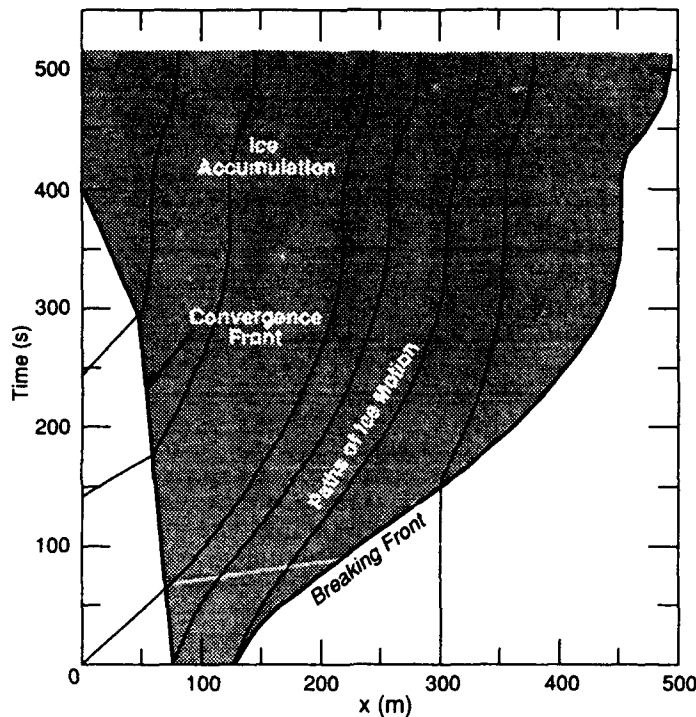


Figure 13. Breaking and convergence front and ice particle motion on the $x-t$ plane that are most consistent with the Connecticut River data.

the $x-t$ plane in Figure 13. The ice motion depicted is that most consistent with the data, $C_{c0} = -0.1$ m/s and $t_{ir}(1 - e_{cr}) = 1.1$ m. The ice particle that departs from site U at 240 s (event time 700 s) represents the thicker ice from upstream that produces a kink in the convergence front trace. As observed, the computed position of the convergence front passes site U moving upstream at 400 s. Figures 4 and 13 both depict developing ice accumulations. However, changing ice and front speeds produce paths with variable slopes that replace the parallel lines of steady motion.

CONCLUSIONS

We developed a kinematic model of ice motion during dynamic river breakup by applying continuity at several fronts in the ice. Breaking, convergence, stoppage and release fronts were described, and relationships were developed between their respective speeds and the changes in unit ice volume and ice discharge across each front. Rapid breaking, stoppage and release front propagation indicate minimal modification of the ice field, while lower speeds correspond to larger changes. The difference in ice speed and unit volume across the convergence front determine the front speed and direction. A convergence front becomes a stoppage front when the ice accumulation speed is zero. Extended breaking front motion at speeds comparable to the ice velocity causes the development of an accumulation while the ice is in motion.

The kinematic model was applied to a dynamic breakup of the Connecticut River using measured ice velocity data at sites both upstream and downstream of a study reach. Important assumptions were that changes in ice and motion conditions occurred only across a front, and that a developing accumulation would have uniform thickness and porosity.

The kinematic analysis supports the relationship described by Ferrick et al. (1992) between ice convergence upstream of a breaking front and front speed. The extremely fast measured breaking front speed that initiated the ice motion in the reach supports the force balance per unit length and the instantaneous support breakup of a river reach in the model of Ferrick and Mulherin (1989). The analysis together with the data provided a hypothetical event sequence of ice processes in the reach. The accumu-

lation length and volume were obtained as functions of the unit accumulation volume, and the mean accumulation unit volume was estimated. Ice and front motions and ice discharge were determined throughout the reach for ranges of accumulation unit volume and initial convergence front speed. The motion simulation most consistent with all the data and observations was presented in the $x-t$ plane. According to this analysis, the ice accumulation formed while in motion, and then arrested, creating a jam.

This kinematic model of ice motion during river breakup represents a new approach to the development of a dynamic model that includes jam formation and release. Static models of ice jam formation neglect both dynamic ice motion and unsteady river flow. In contrast to the static models that are essentially independent of breakup, the kinematic model details the breakup processes. Static models are only applicable when the speed and duration of breaking front motion are small prior to arrest, so that the effect of this motion on the force balance is negligible.

LITERATURE CITED

- Beltaos, S.** (1988) Configuration and properties of a breakup jam. *Canadian Journal of Civil Engineering*, **15**: 685-697.
- Beltaos, S. and B.G. Krishnappan** (1982) Surges from ice jam releases: A case study. *Canadian Journal of Civil Engineering*, **9**: 276-284.
- Billfalk, L.** (1982) Breakup of solid ice covers due to rapid water level variations. USA Cold Regions Research and Engineering Laboratory, CRREL Report 82-3.
- Bourbie, T., O. Coussy and B. Zinszner** (1987) *Acoustics of Porous Media*. Houston, Texas: Gulf Publishing Co.
- Calkins, D.J.** (1978) Physical measurements of river ice jams. *Water Resources Research*, **14**(4): 693-695.
- Doyle, P.F. and D.D. Andres** (1979) Spring breakup and ice jamming on the Athabasca River near Fort McMurray. Transportation and Surface Water Engineering Division, Alberta Research Council, Edmonton, Report SWE-79-05.
- Ferrick, M.G. and N.D. Mulherin** (1989) Framework for control of dynamic ice breakup by river regulation. USA Cold Regions Research and Engineering Laboratory, CRREL Report 89-12.
- Ferrick, M.G.** (1991) Discussion of "Minimization of frazil-ice production by river-flow regulation." by S.C. Jain and R. Ettema, *Journal of Hydraulic Engineering*, American Society of Civil Engineers, **117**(10): 1406-1409.
- Ferrick, M.G., P.B. Weyrick and S.T. Hunnewell** (1992) Analysis of river ice motion near a breaking front. *Canadian Journal of Civil Engineering*, **19**: 105-116.
- Gerard, R. and G. Flato** (1988) Some thoughts on break-up and ice jams. *Proceedings of the 5th Workshop on the Hydraulics of River Ice*, Winnipeg, Manitoba, pp. 225-236.
- Guo, Q.** (1991) Analysis and modeling of the river ice breakup and jamming process and its effect on flooding. Ph.D. Thesis (unpublished), University of Minnesota, September.
- Henderson, F.M. and R. Gerard** (1981) Flood waves caused by ice jam formation and failure. *Proceedings of the IAHR Symposium on Ice*, Quebec City, P.Q., Canada, International Association for Hydraulic Research, 209-219.
- Lighthill, M.J. and G.B. Whitham** (1955) On kinematic waves II. A theory of traffic flow on long crowded roads, *Proceedings Royal Society of London-Series A*, **229**: 317-345.
- Pariset, E., R. Hausser and A. Gagnon** (1966) Formation of ice covers and ice jams in rivers. *Journal of the Hydraulics Division*, American Society of Civil Engineers, **92**(6): 1-24.
- Prowse, T.D., J.C. Anderson and R.L. Smith** (1986) Discharge measurement during river ice breakup. In *Proceedings of the 43rd Eastern Snow Conference*, Hanover, New Hampshire, pp. 55-69.
- Risebro, N.H. and A. Tveito** (1992) A front tracking method for conservation laws in one dimension. *Journal of Computational Physics*, **101**: 130-139.
- Shen, H.T. and Y.C. Chen** (1992) Lagrangian discrete parcel simulation of two-dimensional river ice dynamics. Report 92-9, Dept. of Civil and Environmental Engineering, Clarkson University, Potsdam, New York.
- Uzuner, M.S. and J.F. Kennedy** (1976) Theoretical model of river ice jams. *Journal of the Hydraulics Division*, American Society of Civil Engineers, **102**(9): 1365-1383.
- Williamson, D.** (1989) Unsteady flow aspects of river ice breakup. MS Thesis (unpublished), Dept. of Civil Engineering, University of Alberta, Edmonton.

REPORT DOCUMENTATION PAGE

Form Approved
OMB No. 0704-0188

Public reporting burden for this collection of information is estimated to average 1 hour per response, including the time for reviewing instructions, searching existing data sources, gathering and maintaining the data needed, and completing and reviewing the collection of information. Send comments regarding this burden estimate or any other aspect of this collection of information, including suggestion for reducing this burden, to Washington Headquarters Services, Directorate for Information Operations and Reports, 1215 Jefferson Davis Highway, Suite 1204, Arlington, VA 22202-4302, and to the Office of Management and Budget, Paperwork Reduction Project (0704-0188), Washington, DC 20503.

1. AGENCY USE ONLY (Leave blank)		2. REPORT DATE September 1993	3. REPORT TYPE AND DATES COVERED		
4. TITLE AND SUBTITLE Kinematic Model of River Ice Motion During Dynamic Breakup			5. FUNDING NUMBERS PE: 6.23.734 PR: 4A162734DT08		
6. AUTHORS Michael G. Ferrick, Patricia B. Weyrick and David F. Nelson			PE: 6.27.84A PR 4A762784AT42 TA: CS WU: 001		
7. PERFORMING ORGANIZATION NAME(S) AND ADDRESS(ES) U.S. Army Cold Regions Research and Engineering Laboratory 72 Lyme Road Hanover, New Hampshire 03755-1290			8. PERFORMING ORGANIZATION REPORT NUMBER CRREL Report 93-15		
9. SPONSORING/MONITORING AGENCY NAME(S) AND ADDRESS(ES) Office of the Chief of Engineers Washington, DC 20314-1000			10. SPONSORING/MONITORING AGENCY REPORT NUMBER		
11. SUPPLEMENTARY NOTES					
12a. DISTRIBUTION/AVAILABILITY STATEMENT Approved for public release; distribution is unlimited. Available from NTIS, Springfield, Virginia 22161			12b. DISTRIBUTION CODE		
13. ABSTRACT (Maximum 200 words) We begin a study of the dynamics of ice motion during river breakup by formulating a kinematic model. Ice continuity equations are applied to relate the speeds of a breaking front, convergence front, stoppage front, and release front with the ice discharge and volume per unit surface area (unit volume) on either side of each front. Ice velocity data are obtained from measurements with time made during a dynamic breakup at a pair of sites bounding a reach of the Connecticut River. We simulate the ice and front motion through time for this reach using the kinematic model with the assumptions that accumulation thickness and porosity are uniform, and that changes in the ice conditions and motion occur only at a front. Contrary to the basic assumption of static jam formation, we find that the accumulation develops while the ice is moving, and that jam formation merely represents the arrest of the motion.					
14. SUBJECT TERMS Front tracking Hydraulic modeling			Ice breakup Ice jams	Kinematic model River ice motion	15. NUMBER OF PAGES 24
17. SECURITY CLASSIFICATION OF REPORT UNCLASSIFIED			18. SECURITY CLASSIFICATION OF THIS PAGE UNCLASSIFIED	19. SECURITY CLASSIFICATION OF ABSTRACT UNCLASSIFIED	16. PRICE CODE
20. LIMITATION OF ABSTRACT UL					